Transport dynamics of an interacting binary Bose–Einstein condensate in an incommensurate optical lattice*

Cui Guo-Dong(崔国栋)[a)b)], Sun Jian-Fang(孙剑芳)[a)b)], Jiang Bo-Nan(姜伯楠)[a)b)], Qian Jun(钱 军)[a)†], and Wang Yu-Zhu(王育竹)[a)‡]

[a)] *Key Laboratory for Quantum Optics, Center for Cold Atoms, Shanghai Institute of Optics and Fine Mechanics, Chinese Academy of Sciences, Shanghai* 201800, *China*

[b)] *University of Chinese Academy of Sciences, Beijing* 100049, *China*

(Received 2 April 2013; revised manuscript received 7 May 2013)

We investigate the transport dynamics of an interacting binary Bose–Einstein condensate in an incommensurate optical lattice and predict a novel splitting of a matter wavepacket induced by disorder potential and inter-species interaction. The effect of atomic interaction on the dynamics of the mobile and localized atoms are also studied in detail. We also discuss the behavior of the balanced and inbalanced mixtures in the incommensurate optical lattice.

Keywords: multicomponent Bose–Einstein condensates, Anderson localization, dynamic properties

PACS: 05.30.Jp, 03.75.Hh, 03.75.Mn, 03.75.Kk **DOI:** 10.1088/1674-1056/22/10/100501

In 1958, Anderson predicted the localization and the absence of diffusion of non-interacting quantum particles in the context of transport of electrons in dirty crystals.[1] Anderson localization (AL) can be understood as a ubiquitous interference phenomenon of multiple reflections of a plane wave by disorder. As a single-particle effect, it can be proven that any wavefunction with arbitrary energy is exponentially localized in one-dimensional (1D) cases when it is subjected to disorder.[2,3] In two-dimensional (2D) cases, the situation is similar, but the interference effects are weaker, and a crossover from extended to localized states is shown in finite-size systems.[4] The situation is greatly different in three-dimensional (3D) casse where the Anderson transition occurs at the so-called mobility edge.[5,6] Different from the case of true disorder, there is a metal–insulator transition in 1D cases when an incommensurate lattice is used to mimic disorder.[7,8] AL has been reported in a variety of physical systems, such as light in diffusive media[9,10] and photonic crystals,[11,12] microwaves[13] and sound waves.[14] In recent years, new approaches to the issue came from ultracold atoms confined in disordered potentials. In the context of disordered quantum gases, controllable disorder can be realized with laser speckles and incommensurate optical lattice.[15,16] Therefore the interplay between disorder and interaction can be investigated in detail with unprecedented versatility, tunability, and measurement possibilities.[17] After the milestone of observing AL in a non-interacting matter wave,[18,19] it has been experimentally studied in weak/strong interacting Bose and Fermi gases.[17] Very recently, three-dimensional AL of a non-interacting ultracold atomic gas in a disordered optical speckle potential has been investigated.[20,21]

Nowadays, techniques for producing a binary Bose–Einstein condensate (bBEC) are mature and easy which could be two different hyperfine states of the same species[22] or two different species.[23] Scientists can precisely control scattering length between atoms by Feshbach resonance, which can bring the system into strong interaction regime.[24] Since inter-species interaction is introduced and has a great influence on the dynamics of the matter wave, a bBEC exhibits more novel dynamical features and macroscopic quantum phenomena in contrast to a conventional BEC,[25–29] which has already attracted intensive studies theoretically and experimentally.[30–33] In addition, the effects of temporal and spatial nonlinearities have also been investigated in this context.[34]

In this work, we focus on the transport dynamics of a two-species Bose gas imposed by a state-dependent incommensurate optical lattice which plays a role of disordered potential. As expected, one species of the bBEC subjected to disorder tends to localization, and another disorder-free species exhibits an intriguing splitting of the wavepacket. Unexpectedly, we also demonstrate that, when inter-species interaction is strong enough, a few mobile atoms tend to coexist with localized atoms of the other species. The results presented here show that both disorder and inter-species interaction are of great importance to the transport of the mobile and localized atoms after the trap is turned off.

Now we start from 3D two-species coupled Gross–

*Project supported by the National Natural Science Foundation of China (Grant No. 11104292) and the National Basic Research Program of China (Grant No. 2011CB921504).

†Corresponding author. E-mail: jqian@siom.ac.cn

‡Corresponding author. E-mail: yzwang@mail.shcnc.ac.cn

© 2013 Chinese Physical Society and IOP Publishing Ltd

Pitaevskii (GP) equations given by

$$\begin{aligned} \mathrm{i}\hbar\partial_t \Psi_A &= \left(-\frac{\hbar^2\nabla^2}{2m} + V_{\mathrm{trap}} + V_{\mathrm{dis}} \right. \\ &\quad \left. + g_A|\Psi_A|^2 + g_{AB}|\Psi_B|^2 \right)\Psi_A, \\ \mathrm{i}\hbar\partial_t \Psi_B &= \left(-\frac{\hbar^2\nabla^2}{2m} + V_{\mathrm{trap}} + g_{AB}|\Psi_A|^2 + g_B|\Psi_B|^2 \right)\Psi_B, \end{aligned} \quad (1)$$

where $\Psi_{A,B}$ are the macroscopic wavefunctions of two species, $V_{\mathrm{trap}} = m\left(\omega_\perp^2 r^2 + \omega_z^2 z^2\right)/2$ and V_{dis} are the magnetic trap and the incommensurate optical lattice, respectively. The intra- and inter-species interaction strengths $g_{ii} = 4\pi\hbar^2 a_{ii}/m$, $(i = A, B)$ and $g_{AB} = 4\pi\hbar^2 a_{AB}/m$ are characterized by intra- and inter-species scattering lengths a_{ii} and a_{AB}, respectively. Here we have assumed that only the atoms of the species $\boldsymbol{A}$ are disturbed by the incommensurate optical lattice and both atoms are trapped in a harmonic oscillator potential with the same trap frequencies. Furthermore, we assume that the atoms experience a strong transverse confinement (i.e., $\lambda = \omega_z/\omega_\perp \ll 1$), and one can simplify Eq. (1) into a 1D GP equation

$$\begin{aligned} \mathrm{i}\hbar\partial_t \varphi_A &= \left(-\frac{\hbar^2\partial_z^2}{2m} + V_z + V_{\mathrm{dis}}(z) \right. \\ &\quad \left. + \tilde{g}_A|\varphi_A|^2 + \tilde{g}_{AB}|\varphi_B|^2 \right)\varphi_A, \\ \mathrm{i}\hbar\partial_t \varphi_B &= \left(-\frac{\hbar^2\partial_z^2}{2m} + V_z + \tilde{g}_{AB}|\varphi_A|^2 + \tilde{g}_B|\varphi_B|^2 \right)\varphi_B, \end{aligned} \quad (2)$$

with the axial harmonic trap $V_z = m\omega_\perp^2\lambda^2 z^2/2$, the reduced 1D effective interaction strengths $\tilde{g}_{ii} = g_{ii}/(2\pi l_\perp^2)$ and $\tilde{g}_{AB} = g_{AB}/(2\pi l_\perp^2)$ ($l_\perp = \sqrt{\hbar/(m\omega_\perp)}$ is the oscillation length in the transverse plane). Furthermore, when the units of length, energy, and time are chosen as $l_\perp$, $\hbar\omega_\perp$, and $\omega_\perp^{-1}$, respectively, one can investigate the wavepacket dynamics in 1D using the following dimensionless GP equations

$$\begin{aligned} \mathrm{i}\partial_t \varphi_A &= \left(-\frac{\partial_z^2}{2} + \frac{1}{2}\lambda^2 z^2 + V_{\mathrm{dis}}(z) \right. \\ &\quad \left. + \mu_A|\varphi_A|^2 + \mu_{AB}|\varphi_B|^2 \right)\varphi_A, \\ \mathrm{i}\partial_t \varphi_B &= \left(-\frac{\partial_z^2}{2} + \frac{1}{2}\lambda^2 z^2 + \mu_{AB}|\varphi_A|^2 + \mu_B|\varphi_B|^2 \right)\varphi_B, \end{aligned} \quad (3)$$

where $\mu_{ii} = 2Na_{ii}/l_\perp$ and $\mu_{AB} = 2Na_{AB}/l_\perp$ are dimensionless 1D effective intra- and inter-species interaction strengths, respectively. In addition, the density of each component is normalized to the ratio of its atom number to the total number N_{tot}. The incommensurate optical lattice $V_{\mathrm{dis}}(z) = s_1\sin^2(k_1 z) + s_2\beta^2\sin^2(k_2 z)$ is used to mimic disorder, where $s_{1,2}$ are the lattice depths and $\beta = k_1/k_2$, k_1 and k_2 are the wavenumbers of the primary and secondary lattices, respectively. The above equations can be solved numerically by the split-step spectral method.[35] We firstly obtain a ground state by solving Eq. (3) without V_{dis}, then turn off the axial harmonic trap and propagate this wavepacket in the incommensurate optical lattice.

Now we turn to present numerical results and discuss the behavior of the wavepackets in the incommensurate optical lattice. Initially, we only consider a balanced mixture with equal atom numbers, here, i.e., $N_A = N_B = 5\times10^4$. The transverse and axial trap frequencies are $\omega_\perp = 2\pi\times100$ Hz and $\omega_z = 2\pi\times5$ Hz, respectively. Thus the tight confinement in x and y directions ensures a cigar-shaped quasi-1D BEC. The wavelengths of the primary and secondary lattices are 1032 nm and 862 nm,[18] respectively, and the primary lattice depth $s_1 = 10E_{\mathrm{r}}$ is fixed (E_{r} is the photon recoil energy of the primary lattice). Thus one can control the disorder strength only by adjusting the depth of the secondary lattice. Because we are interested in the effect of AL on the diffusion of the matter wavepacket, we will choose appropriate parameters for the appearance of the localization of the species $\boldsymbol{A}$ in our calculations.

We plot the transport process of the weakly interacting binary BEC in a natural symmetric case with identical atomic interaction strengths $\mu_A = \mu_B = \mu_{AB} = 1$ in Fig. 1. In this special case, the initial density profiles of both species are the same because of the identical scattering lengths between atoms. In the situation of no incommensurate optical lattice and inter-species interaction, they will spread freely simultaneously. However, one can observe remarkably the localization of the wavepacket of the species $\boldsymbol{A}$ after adiabatically loading the disordered potential in 100 ms. After that moment, the atoms of the species $\boldsymbol{A}$ are localized in distinct lattice sites around the center of the initial BEC (see Figs. 1(a) and 1(b)), which exhibits a clear signature of localization. Here we have chosen an appropriate value of lattice depth of the secondary lattice which is favorable to the localization. The incommensurate optical lattice plays an important role as disorder in the diffusion of the localized atoms. The wavefunction of the species $\boldsymbol{A}$ is scattered by the incommensurate optical lattice and the scattered waves interfere destructively from each other. Finally the diffusion of the wavefunction is terminated and the atoms are localized in distinct sites. Since the spatial range of the ground-state wavefunction is much larger than the lattice constant of the primary lattice, many localized states appear in this situation.[16,36]

Interestingly, we also find a striking splitting of the wavepacket of the species $\boldsymbol{B}$ as clearly shown in Fig. 1(c), which happens after 100 ms. The atom number decreases rapidly and few atoms occupy in the sites around the center at last. It indicates that the localized atoms of the species $\boldsymbol{A}$ push out the mobile atoms of the species $\boldsymbol{B}$. When we look at the final profiles of both species (see Figs. 1(b) and 1(d)),

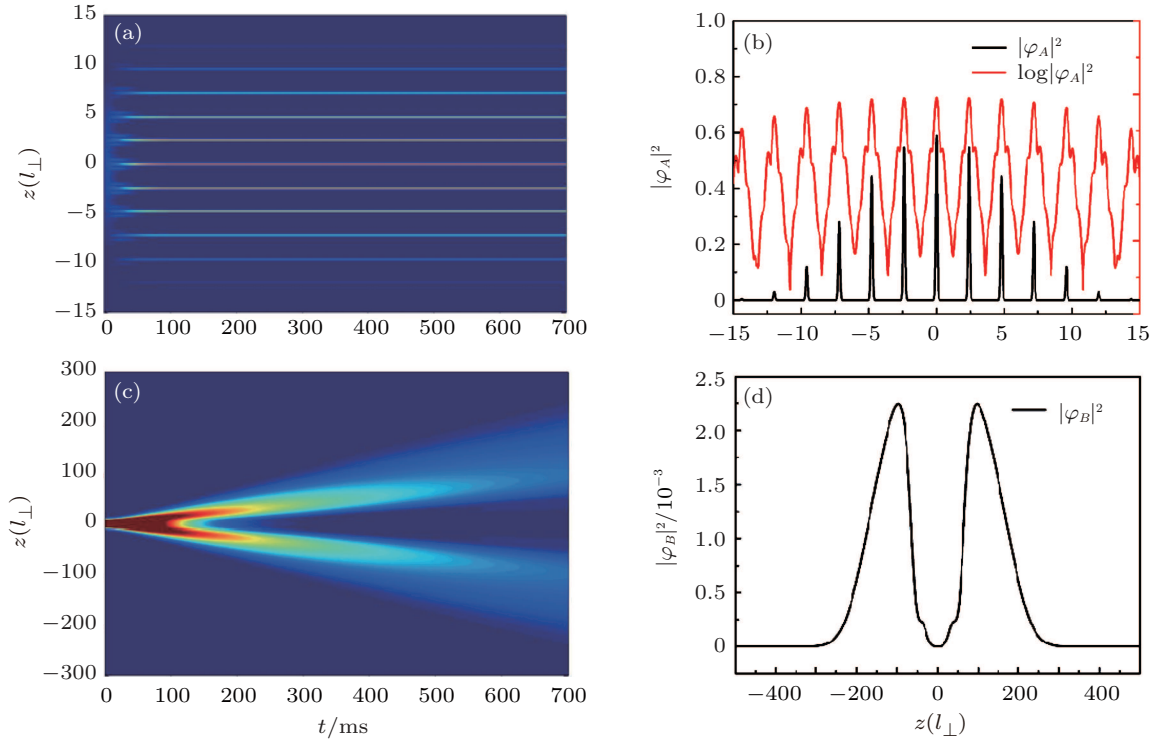


Fig. 1. (color online) Transport dynamics and final density profiles of a binary BEC. Upper panels (a) and (b): the localized species $\boldsymbol{A}$, lower panels (c) and (d): the mobile species $\boldsymbol{B}$. We have set $\mu_A = \mu_B = \mu_{AB} = 1$ and $s_2 = 3E_r$.

we find sharp peaks in the distribution of the species $\boldsymbol{A}$ in a small region around the center and a symmetric double-hump of the species $\boldsymbol{B}$, which illustrates definitely the localization and splitting of the respective wavefunctions.

It should be noted that it is not a coincidence that the localization and the splitting happen simultaneously. Intuitively, one can understand the physics as follows. At first, both species begin to spread along the z direction when the trap is turned off, and then the atoms of the species $\boldsymbol{A}$ experience the incommensurate optical lattice until they are completely localized after 100 ms. Because of repulsive interaction between the atoms of different species, the mobile species at the center will be repelled by the localized atoms, which results in the final splitting with a double-hump profile. Another important feature is the irregular shape of each hump. In fact, during the expansion of the atoms, the interaction energy translates to kinetic energy that determines the velocity of the diffusing atoms and density distribution of the atomic wavepacket. At the center, repelled by the localized atoms nearby, the mobile atoms with strong interaction energy translate to kinetic energy that will contribute rapid expansion toward the two wings. On the contrary, few localized atoms interacted with the mobile atoms in both wings, and then the interaction energy contributes little. Therefore the mobile atoms in the central zone diffuse more rapidly than those on the edge of the hump, and finally the humps have a steep slope close to the center.

In the above discussion we have interpreted splitting of a disorder-free species' wavepacket qualitatively, now let us give a quantitative analysis on the novel splitting. In fact, the diffusion of the spreading atomic clouds can be characterized by its spatial extension (root-mean-size, RMS) $\Delta r_{A,B} = \sqrt{\int_{-\infty}^{+\infty} z^2 |\varphi_{A,B}|^2 \mathrm{d}z}$ and positive average momentum $\bar{p}_B = \int_0^{+\infty} p|\varphi_B|^2 \mathrm{d}p$. We also introduce central fraction $f_c^{A,B} = \int_{-z_0}^{z_0} |\varphi_i|^2 \mathrm{d}z$ and peak-to-peak distance d to describe the escape of the atoms from the center and the departing humps. Because of the symmetric distribution of the wavepacket, only the component in the positive direction should be considered. Here we have defined the central fraction as the ratio of the atom number in the zone with $1/e$ width (z_0) of the initial BEC to the total atom number. As shown in Figs. 2(a) and 2(b), one can observe that $f_c^{(A)}$ decreases slightly to a constant and Δr_A remains unchanged after a rapidly increase in a short time, which indicates the appearance of the localization. The other species exhibits different behavior that cannot be roughly explained by the localization or ballistic expansion. The RMS of the species $\boldsymbol{B}$ is different from that of the localized one and it increases linearly during the evolution as shown in Fig. 2(b). However, the mobile atoms do not experience ballistic expansion because its central fraction reduces to nearly zero that indicates the escape of the mobile atoms along the z direction. During the expansion, the external potential and intrinsic interaction energies experienced by the mobile atoms will translate to their kinetic energy and results in the acceleration of the disorder-free atoms (see also Fig. 3(c)). Besides that, the peak-to-peak distance d can also

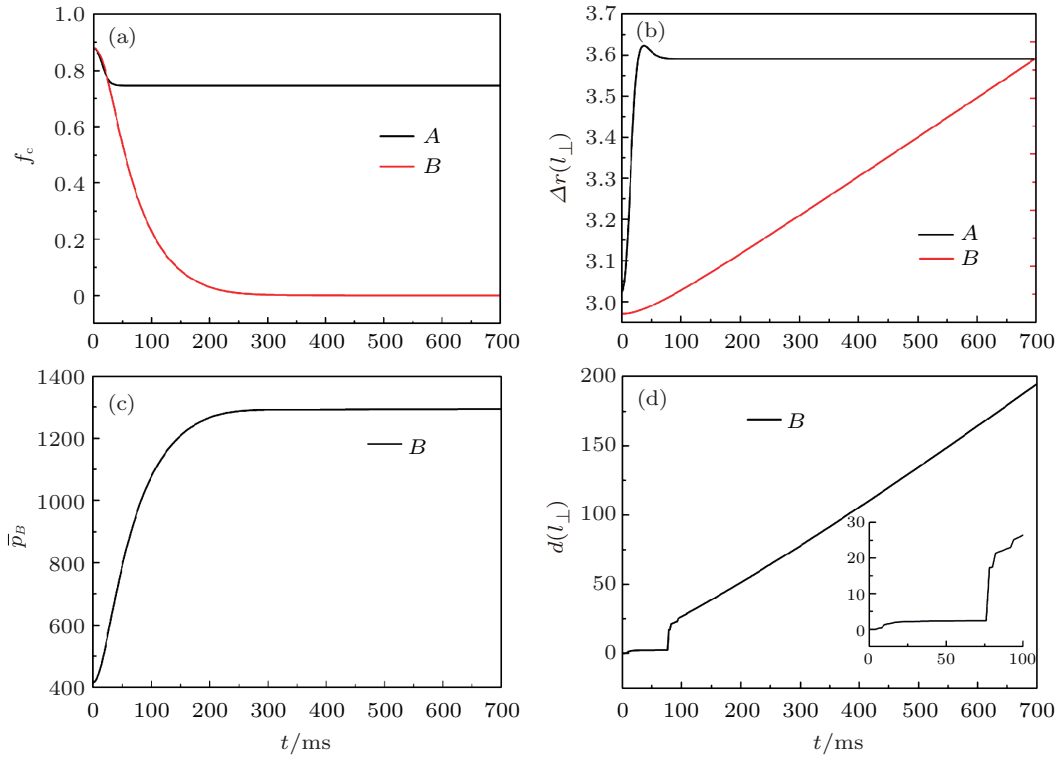


Fig. 2. (color online) (a) Central fraction, (b) RMS, (c) positive average momentum, and (d) peak-to-peak distance (the initial stage is highlighted in the inset). The values are distracted from Fig. 1.

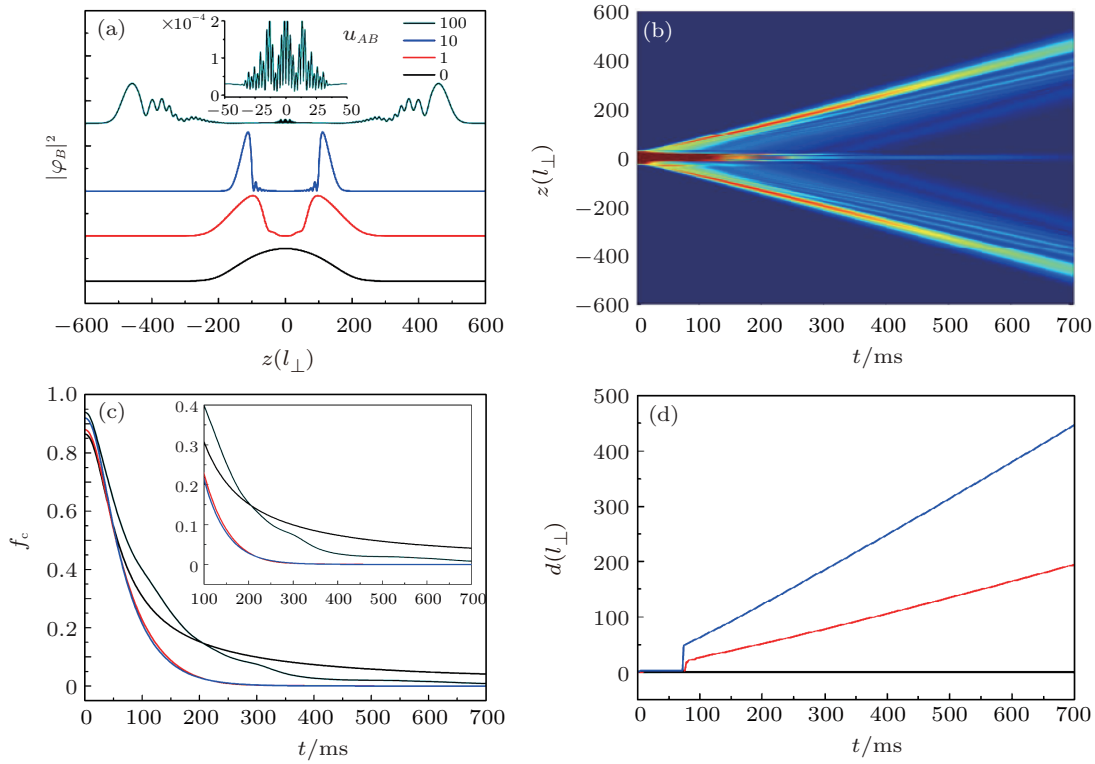


Fig. 3. (color online) (a) Final density profiles of the species $\boldsymbol{B}$ corresponding to different inter-species interaction strengths at 700 ms (the inset shows the density in the center at $\mu_{AB} = 100$). (b) Transport dynamics of the wavepacket of the mobile species for inter-species interaction strengths $\mu = 100$ during the evolution time $t = 700$ ms. (c) Central fraction of species $\boldsymbol{B}$ (the evolution after 100 ms is presented in the inset). (d) Peak-to-peak distance. The parameters are the same as that in Fig. 2 except the inter-species interaction.

illustrate the wavepacket splitting of the mobile species (see also Fig. 2(d)). Initially, all the atoms expand after turning off the trap and d remains zero. Once the atoms in the state $\boldsymbol{A}$ are localized when the disorder potential is completely loaded, the atoms in the disorder-free state $\boldsymbol{B}$ around the center are accelerated due to the repulsion by the localized atoms. Specially,

there is an abrupt jump when we look at the time evolution of the peak-to-peak distance, which implies the starting point of the wavepacket splitting. After that moment, the peak-to-peak distance increases linearly that means two humps of the wavepacket depart from each other.

So far, we have demonstrated that the splitting of the disorder-free species appears after the localization of the species experienced by the incommensurate optical lattice. We can hereby say that the incommensurate optical lattice plays an indispensable role in the transport dynamics of the binary BEC. It has been reported in our previous work that the localized atoms can occupy more sites when interaction becomes strong.[37] Now we are in position to explore the effect of the inter-species interaction on this novel disorder-induced splitting. In Fig. 3, the diffusion dynamics of the species $\boldsymbol{B}$ is shown at different inter-species interaction strength. For comparison, we also provide the result of the non-interacting gas in Fig. 3(a), which indicates ballistic expansion as expected. Even in the situation of weak inter-species interaction, a perfect splitting can be realized when the whole wavepacket is split into two separated wings. One can also find that a strong inter-species interaction aggravates the separation remarkably. This result is expected because strong repulsive interaction energy will be translated to kinetic energy greatly and contributes a rapid diffusion of the mobile species. It is strikingly unexpected, however, in the strong interaction limit as shown in Fig. 3(b), a certain amount of the flying atoms are still trapped at the center. Since the species $\boldsymbol{A}$ will be localized in a short time, we can regard it as a static component approximately. Hence one can treat the interaction term in the GP equation of the species $\boldsymbol{B}$ (Eq. (3)) as a time-independent effective potential similar to the external potential, i.e., $\mu_{AB}|\varphi_A(z,t)|^2 \longrightarrow V_{\text{eff}}(z)$.[38] Now we can explain the coexistence of the mobile and localized species around the center as follows. Remember that the quasi-static effective potential $V_{\text{eff}}(z)$ should have the same comb-like structure as the density distribution of the localized atoms (see Fig. 1(b)). When μ_{AB} is large enough, $V_{\text{eff}}(z)$ can be regarded as a comb-like barrier which can prohibit the spread of a small amount of the atoms with decreasing kinetic energy and trap them in the valleys in the central zone. That is why a few atoms always occupy the sites at the center in Figs. 3(a)–3(c) when $\mu_{AB} = 100$. Moreover, a stronger μ_{AB} results in a longer distance d between the peaks at the initial stage of the splitting, and two humps of the wavepacket will be widely separated. This is because more interaction energy is translated into the kinetic energy.

In the above discussion, we only consider the balance mixture, that is to say, the atom numbers of each species are the same. Below we further investigate the situation of inbalance mixture with special focus on the impact on the wavepacket splitting of the disorder-free species. We choose three cases of the mixture with $N_A/N_B = 1:3, 1:1, 3:1$ and fix the total atom number $N_{\text{tot}} = 10^5$. The final density profiles of the component $\boldsymbol{B}$ are shown in Fig. 4(a). It should be noted that the renormalized envelopes differ from each other because the doping ratio is different. It is quite clear that the separation of the two humps is strengthened when more localized atoms join in the mixture. Similar to the balanced mixture, we also use similar physical parameters to quantitatively analyze the behavior of mobile species (see Figs. 4(b)–4(d)). The peak-to-peak distance abruptly increases from zero to a certain value at about 100 ms, which indicates the beginning of the splitting. Subsequently the distance keeps the tendency of linear growth no matter how many of the atoms $\boldsymbol{A}$ are mixed. And our calculation finds positive correlations between the slope of the peak-to-peak distance and the number of the localized species, which is consistent with the COM's evolution in Fig. 4(d). In addition, average positive momentum tends to a constant after the appearance of the localization, although the final values of $\bar{p}_B$ is different. As is well known, once the trap is turned off, the velocity of escaped atoms is determined by the interaction energy when they are trapped. Assuming that the atoms $\boldsymbol{A}$ are almost static and trapped in the center zone, one can realize that the inter-species interaction strengths and the number of the localized species have a significant contribution to the total interaction energy of the flying atoms. Since a_{AB} is fixed, the number of the species $\boldsymbol{A}$ is only related to the potential energy before the complete separation between two species. As a consequence, after the localization of the species $\boldsymbol{A}$ at about 100 ms, the flying atoms are repelled by the localized atoms and the inter-species interaction energy subject to the atoms $\boldsymbol{B}$ will translate to the kinetic energy. For a mixture with more atoms of the species $\boldsymbol{A}$, the mobile atoms are pushed more heavily along to the propagation direction and will reach a larger value of a_{AB}. Once most of the flying atoms leave the zone occupied by the localized atoms, the inter-species interaction energy has little influence on their movement, the mobile species will probably fly at a constant velocity. This explains well the linear growth of d and z_{c} and different final values of these parameters.

In summary, we have described the transport of a binary BEC in an incommensurate optical lattice, and predicted the novel splitting of the disorder-free species with two separated dumps. We attribute the separation to the inter-species scattering between the atoms of both species and the external incommensurate optical lattice. The behavior of the bBEC has been also analyzed in detail and relevant parameters are calculated, such as peak-to-peak distance, central fraction, and so on. We hope that this work may provide new insights on the dynamics of multi-component disordered quantum gases.

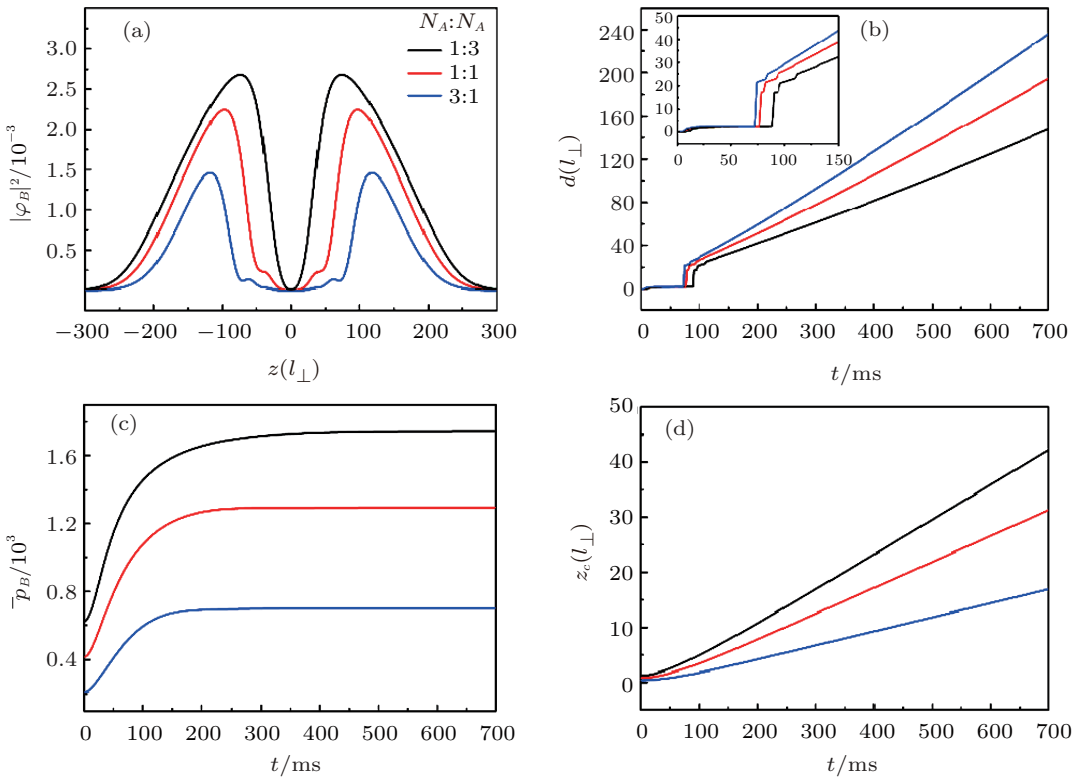


Fig. 4. (color online) The splitting of the species $\boldsymbol{B}$ in an imbalanced mixture: renormalized density profile (a), peak-to-peak distance (b), average positive momentum (c), and positive center-of-mass (COM) $z_c = \int_0^{+\infty} z|\varphi_B|^2 \mathrm{d}z$ (d) at different doped proportion $N_A/N_B = 1:3, 1:1, 3:1$. The parameters are the same as those in Fig. 1.

References

[1] Anderson P W 1958 *Phys. Rev.* **109** 1492
[2] Mott N F and Twose W D 1961 *Adv. Phys.* **10** 107
[3] Borland R E 1963 *Proc. R. Soc. A* **274** 529
[4] Abrahams E, Anderson P W, Licciardello D C and Ramakrishnan T V 1979 *Phys. Rev. Lett.* **42** 673
[5] Ioffe A F and Regel A R 1960 *Prog. Semicond.* **4** 237
[6] Mott N F 1967 *Adv. Phys.* **16** 49
[7] Harper P G 1955 *Proc. Phys. Soc. A* **68** 874
[8] Aubry S and André 1980 *Ann. Israel Phys. Soc.* **3** 133
[9] Wiersma D S, Bartolini P, Lagendijk A and Righini R 1997 *Nature* **390** 671
[10] Störzer M, Gross P, Aegerter C M and Maret G 2006 *Phys. Rev. Lett.* **96** 063904
[11] Schwartz T, Bartal G, Fishman S and Segev M 2007 *Nature* **446** 52
[12] Lahini Y, Avidan A, Pozzi F, Sorel M, Morandotti R, Christodoulides D N and Silberberg Y 2008 *Phys. Rev. Lett.* **100** 013906
[13] Chabanov A A, Stoytchev M and Genack A Z 2000 *Nature* **404** 850
[14] Hu H, Strybulevych A, Page J H, Skipetrov S E and van Tiggelen B A 2008 *Nat. Phys.* **4** 945
[15] Lewenstein M, Sanpera A, Ahufinger V, Damski B, Sen A and Sen U 2007 *Adv. Phys.* **56** 243
[16] Lye J E, Fallani L, Modugno M, Wiersma D S, Fort C and Inguscio M 2005 *Phys. Rev. Lett.* **95** 070401
[17] Sanchez-Palencia L and Lewenstein M 2010 *Nat. Phys.* **6** 87
[18] Roati G, D'Errico C, Fallani L, Fattori M, Fort C, Zaccanti M, Modugno G, Modugno M and Inguscio M 2008 *Nature* **453** 895
[19] Billy J, Josse V, Zuo Z, Bernard A, Hambrecht B, Lugan P, Clément D, Sanchez-Palencia L, Bouyer P and Aspect A 2008 *Nature* **453** 891
[20] Kondov S S, McGehee W R, Zirbel J J and DeMarco B 2011 *Science* **334** 66
[21] Jendrzejewski F, Bernard A, Müller K, Cheinet P, Josse V, Piraud M, Pezze L, Sanchez-Palencia L, Aspect A and Bouyer P 2012 *Nat. Phys.* **8** 398
[22] Myatt C J, Burt E A, Ghrist R W, Cornell E A and Wieman C E 1997 *Phys. Rev. Lett.* **78** 586
[23] Thalhammer G, Barontini G, De Sarlo L, Catani J, Minardi F and Inguscio M 2008 *Phys. Rev. Lett.* **100** 210402
[24] Chin C, Grimm R, Julienne P and Tiesinga E 2010 *Rev. Mod. Phys.* **82** 1225
[25] Zhou Y, Huang G X, Ma X D and Ma Y L 2006 *Chin. Phys.* **15** 1871
[26] Hao Y J and Liang J Q 2006 *Chin. Phys.* **15** 1161
[27] Ao S M and Yan J R 2006 *Chin. Phys.* **15** 296
[28] Zhan M S, Wen L H, Liu M, Kong L B and Chen A X 2005 *Chin. Phys.* **14** 690
[29] Wang D L, Tang Y and Yan X H 2004 *Chin. Phys.* **12** 203
[30] Papp S B, Pino J M and Wieman C E 2008 *Phys. Rev. Lett.* **101** 040402
[31] Pu H and Bigelow N P 1998 *Phys. Rev. Lett.* **80** 1134
[32] Pu H and Bigelow N P 1998 *Phys. Rev. Lett.* **80** 1130
[33] Zhou X J, Li W D, Chen X Z and Wang Y Q 2002 *Chin. Phys. Lett.* **19** 1581
[34] Wang D S, Hu X H and Liu W M 2010 *Phys. Rev. A* **82** 023612
[35] Press W H, Teukolsky S A, Vetterling W T and Flannery B P 2007 *Numerical Recipes: The Art of Scientific Computing*, 3rd edn. (Cambridge: Cambridge University Press)
[36] Modugno G 2010 *Rep. Prog. Phys.* **73** 102401
[37] Xu Z, Duan Y F, Zhou S Y, Hong T and Wang Y Z 2009 *Chin. Phys. Lett.* **26** 090303
[38] De Nicola S, Malomed B A and Fedele R 2006 *Phys. Lett. A* **360** 164